Statistics of worms and overlap loops in square lattice dimer model

A Thesis

submitted to
Indian Institute of Science Education and Research Pune
in partial fulfillment of the requirements for the
BS-MS Dual Degree Programme

by

Anoop Raj

Indian Institute of Science Education and Research Pune
Dr. Homi Bhabha Road,
Pashan, Pune 411008, INDIA.

, 2021

Supervisor: Dr Kedar Damle

Certificate

This is to certify that this dissertation entitled 'Statistics of worms and overlap loops in square lattice dimer model' towards the partial fulfilment of the BS-MS dual degree programme at the Indian Institute of Science Education and Research, Pune represents study/work carried out by Anoop Raj at Indian Institute of Science Education and Research under the supervision of Dr Kedar Damle, Professor, Department of Physics, TIFR Mumbai during the academic year 2020-2021.

Kedar Damle

Dr Kedar Damle

Committee:

Dr Kedar Damle Kedar Damle

Dr Deepak Dhar

Dedicated to my grand father

Declaration

I hereby declare that the matter embodied in the report entitled Statistics of worms and overlap loops in square lattice dimer model are the results of the work carried out by me at the Department of Physics, Indian Institute of Science Education and Research, Pune, under the supervision of Dr Kedar Damle, TIFR Mumbai and the same has not been submitted elsewhere for any other degree.

Anoop Raj

Acknowledgments

I want to express my deepest gratitude to my supervisor Prof. Kedar Damle for allowing me to work under his guidance and constantly supporting me throughout the duration of this project. I am also extremely grateful to my co-supervisor Prof. Deepak Dhar for his guidance and advice throughout my IISER life.

I feel myself blessed to be mentored by them. Their advice and insights throughout the duration of this project has helped me learn more about this subject and improve my work.

I also want to thank all the faculty at IISER Pune for helping me grow as a student. I would also like to acknowledge INSPIRE scholarship by DST, Government of India, for supporting me as a BS-MS student.

I want to thank my friends for always being there for me and making my college life exciting. I would also like to thank my cricket team mates 'Silent Warrios' for making my life more joyful and for all the IPL memories.

Finally but most importantly I would like to thank my ever-supportive family for all their love and care.

Abstract

In this thesis, we discuss the non-intersecting loops formed by super-posing two random dimer configurations and how these are similar to contour lines of random gaussian surfaces. We specifically use a fully packed dimer cover of a square lattice and numerically try to find the exponents characterizing the distribution of subloops formed when two random dimer configurations are over-lapped.

To generate a random dimer configuration we use the worm algorithm. We specify what the worm algorithm is and its relation to a random walk. We look at the probability distribution of the length of worms generated. To know more about the geometry of the worm, we look at the probability distribution of subloops that a worm breaks into. We find that these worms are non-markovian in nature and their subloops distribution show behaviour similar to subloops generated in random dimer overlap.

Contents

Chapter 1

Introduction

The goal of Statistical Mechanics is to extract knowledge about the macroscopic observable starting from the microscopic level. There are several models whose exact solution has helped to understand the physics of different systems. One of those models is the Dimer model. We begin by defining the problem on a two-dimensional square lattice and work in a finite scale and take the thermodynamic limit in the end.

The Dimer Model was introduced for the first time by Fowler and Rushbrooke [1], in 1937. The first breakthrough came during the 1960s, when the partition function of the dimer model was calculated by Kasteleyn [2], and independently by Temperley and Fisher [3], and dimer-dimer correlation function was calculated by Fisher and Stephenson [4]. Dimer models since then have been used to study many different system such as Ising model [5], frustrated spin system, resonating valence bond system [6], and after the interpretation the dimer model in terms of height field ([7],[8],[9],[10],[11]), it has been used to study random gaussian surfaces.

We will use the idea of height field in the case of dimer model on a square lattice and see how these are related to random gaussian surfaces. The random height field is a set of correlated random variables, one for each site of the lattice. To achieve the random dimer configuration, we use the Monte Carlo worm algorithm. The Worm Algorithm is an efficient way of implementing non-local updates in the system. The properties of the worm constructed during the algorithm are itself interesting. Statistical properties of worm in triangular and kagome lattice have been studied [12].

In Chapter 2, we introduce the dimer model on the square lattice and see how we can define height function on it. We then look at the distribution of subloops formed, when two random dimer configurations are overlapped and the exponents characterizing these subloops' distribution.

In Chapter 3, we look at the statistical properties of the worm generated by the worm algorithm on a fully packed dimer configuration on a square lattice. We specifically look at the distribution of length of the worm and see how it can be seen as a random walk. We will also look at the distribution of subloops that a worm breaks into, which can be visualized when two successive dimer configurations are overlapped.

Chapter 2

Dimer Model

2.1 Dimer Model and Tiling

Let's consider a Graph,

$$G = (V, E),$$

where V is vertices and E is edges and G is planar, finite, with no loops and multiple edges.

A dimer is like a diatomic molecule whose endpoints sit on two adjacent vertices of a graph. A perfect matching or dimer covering of graph G is a set of all edge e$\subset$E such that each vertex is exactly occupied by one dimer. In the physics literature, these perfect matchings are called valid dimer covers (σ). We assign weight $w(e)$ to each edge then,

$$W(\sigma) = \prod_{e \epsilon \sigma} w(e),$$

where W(σ) is the weight of Configuration(σ). Then, Partition function of Graph Z(G) is

$$Z(G) = \sum_{\sigma} W(\sigma) = \sum_{\sigma} \prod_{e} w(e). \tag{2.1}$$

If w(e)=1 $\forall$ e, then Z(G) is the total number of dimer configurations possible.

To define the tiling model, consider planar embedding of graph G, $G^{\hat{*}}$ (Fig 2.2), whose vertices are the centre of the face of graph G. A tile of $G^{\hat{*}}$ is the polygon that forms when

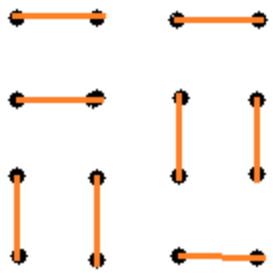

Figure 2.1: Dimer configuration on a subgraph of square lattice

the edges of $\hat{G^*}$ that are intersecting the dimer on graph G are omitted, and this is done such that there are no holes and overlaps. (Fig 2.3).

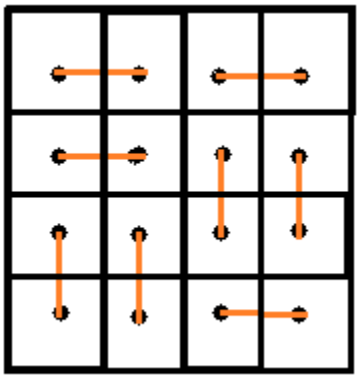

Figure 2.2: Planar embedding of Graph G, solid black lines represents the edges of dual graph $\hat{G^*}$

For a given dimer configuration, once the tiling is done, we can define the height function on the vertices (marked by red dots in Fig 2.3) of this tiling configuration.

2.2 Height Function

To define the height function, we assign two colours, green and white, for the faces of $\hat{G^*}$ such that adjacent to white face; all faces are green and vice versa. After doing this, we

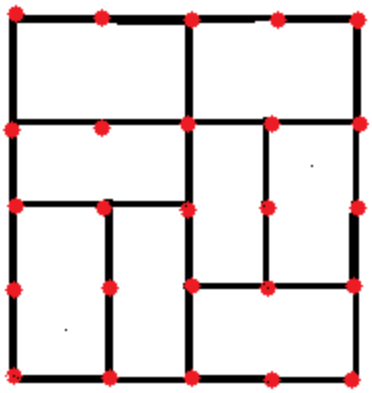

Figure 2.3: Tiling of Graph G on its dual graph $\hat{G^*}$

orient the green faces counter-clockwise and white faces clockwise (Fig 2.4). Now, height

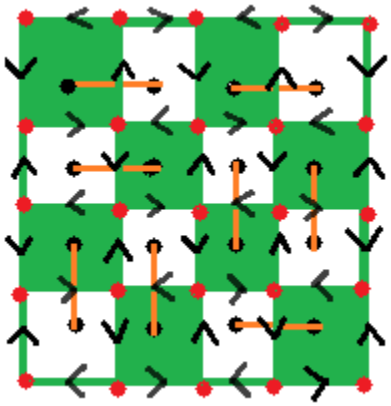

Figure 2.4: Faces of Graph $\hat{G^*}$ coloured and oriented

function is defined inductively on vertices of $\hat{G^*}$ as follows:

- Fix height at one of the vertex to be zero, h(v) =0.
- With respect to v, height is defined at all other vertex according as:
  - h(v)-h(u) = 1 if edge is oriented from u to v, where u and v are vertices of $\hat{G^*}$.
  - h(v)-h(u) = -1 if edge is oriented from v to u.

– h(v)-h(u) = -3 or +3 if edge is oriented from (u to v) or(v to u) and edges are crossing the dimer on the Graph G.

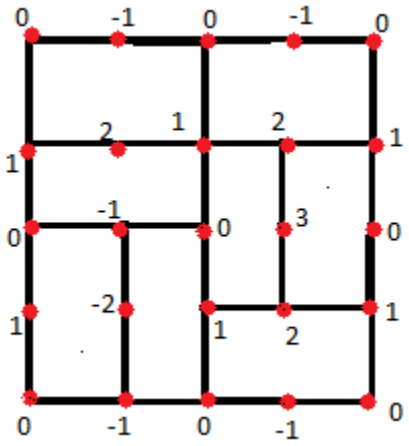

Figure 2.5: Height function defined on vertices of graph $G^{\hat{*}}$ which can also be seen as height defined on the faces of Graph G

As we have seen while inductively defining the height function of G, we needed to orient the edges of dual graph $G^{\hat{*}}$. We can orient the edges on Graph G and define the height function on the face of it. Let's denote the set of oriented edges of Graph G by E, then flow f is a real valued function defined on E i.e. we assign f(u,v) for each directed edge (u,v) of E. Define divergence $divf(u)$, a real valued function defined on vertices V that gives the difference between total inflow and outflow at a given vertex,

$$\forall u \epsilon V, \quad divf(u) = \sum_{v \sim u} f(u,v) - \sum_{v \sim u} f(v,u). \tag{2.2}$$

We separate the vertices into green (Gr) and white (W) such that V = W ∪ Gr. Every dimer configuration(σ) of G defines a unit flow from white to green as defined:

- f^{σ}= 0 for all directed edges which do not belong to configuration σ.
- for edge (w,gr) ϵ σ , $f^{\sigma}(w, gr) = 1$ and $f^{\sigma}(gr, w)$ =0.

Since, In perfect matching (σ), every vertex is incident to one dimer, the flow f has divergence 1 at the white vertex and -1 at the green vertex according to our convention.

$$\begin{aligned}
&\forall\ gr\ \epsilon\ Gr,\ div^{\sigma}(gr) = \sum_{w\sim gr} f(gr,w) - \sum_{w\sim gr} f(w,gr) = -1,\\
&\forall\ w\ \epsilon\ W,\ div^{\sigma}(w) = \sum_{gr\sim w} f(w,gr) - \sum_{gr\sim w} f(gr,w) = 1.
\end{aligned} \tag{2.3}$$

Let B be a reference perfect matching of G with flow f^B, then for any other matching A with flow f^A, $f^A - f^B$ depicts the flow of overlapped configuration of A and B and is divergence-free.

$$\begin{aligned}
\forall\ gr\ \epsilon\ Gr,\ div(f^A - f^B)(gr) &= \sum_{gr\sim w}(f^A(gr,w) - f^B(gr,w)) - \sum_{gr\sim w}(f^A(w,gr) - f^B(w,gr)),\\
&= div\ f^A(gr) - div\ f^B(gr) = (-1) - (-1) = 0.
\end{aligned} \tag{2.4}$$

and similarly for white vertices.

Height function h^A is defined on faces of G as:

- select a face f_o of G and set $h^A(f_o)$ =0.
- Now, for any other face f_i, consider a edge path α on dual graph G^*. The path α had crossed many edges $(u_i, v_i), i = 1\ to\ k$ of Graph G , then $h^A(f_1) - h^A(f_k)$ is the total flux of $f^A - f^B$ across α,

$$h^A(f_1) - h^A(f_o) = \sum_i (f^A(gr,w) - f^B(gr,w)) - \sum_{gr\sim w}(f^A(w,gr) - f^B(w,gr). \tag{2.5}$$

Height function is well defined up to a choice of base face and a reference matching B because $f^A - f^B$ is divergence-free (Eq 2.4).

2.3 Random Gaussian Surfaces

The study of the random gaussian surfaces has helped us understand many different areas of science such as membrane in biology, growth of crystalline surface to the strings of string theory. The fluctuations in these systems, like thermal in the case of membrane, quantum in the case of string, are due to random gaussian surface and determined by the stiffness

K. However, there are certain exponents of random gaussian surfaces that are independent of stiffness and mainly depend on the contour loops. Using analytical scaling arguments, a relation was derived relating several exponents such as D_f (fractal dimension of contour loop), ζ roughness, etc [13].

A random gaussian surface is given by height function h(r), r ϵ $\mathbb{R}^2$, and h(r) ϵ $\mathbb{R}^2$ (in case of membrane and rough surface). Probability distribution of height function is given by Boltzmann factor $e^{-f_\zeta(h)}$, where f_ζ is gaussian free energy,

$$f_\zeta(h) \;=\; \frac{K}{2}\int^{\frac{1}{a}} d^2q(q^2)^{1+\zeta}|\tilde{h}(q)|^2, \tag{2.6}$$

where, K=stiffness, $\tilde{h}$(q)= fourier transform of height function, ζ = roughness exponent, $\frac{1}{a}$ = large momentum cutoff provided by lattice spacing.

Let G(r) be the contour correlation function that measures the probability of 2 points lying on the same loop separated by r,

$$G(r) \sim \frac{1}{r^{2x_1}}, \quad for\ large\ r. \tag{2.7}$$

It was shown that exponent x_1 is universal, independent of ζ and $x_1 = \frac{1}{2}$.

Probability that contour lines of length s passes through a fixed point on a plane is denoted by $\tilde{P}(s)$ and it follows a power law

$$\tilde{P}(s) \;\sim\; \frac{1}{s^{\tau-1}}. \tag{2.8}$$

Scaling relation between various exponent that characterize the contour loop is as:

[13]

$$\begin{aligned} D_f \;&=\; 2 - x_1 - \frac{\zeta}{2}, \\ \tau - 1 \;&=\; \frac{2-\zeta}{2 - x_1 - \frac{\zeta}{2}}, \end{aligned} \tag{2.9}$$

where, D_f is the fractal dimension of the loop, ζ is a measure of roughness, x_1 is the universal exponent of defect-antidefect correlation function, τ is the scaling exponent of distribution

of contour lengths.

2.4 Distribution of loops of Overlap Dimer configuration

When we super-impose two dimer configurations, we get a set of non-intersecting loops. As we have seen in Sec 2.2, we can define the height function on this overlapped dimer configuration, and then we can study these loops in terms of gaussian fixed point of the coarse-grained height field. These loops can be seen as contour lines of gaussian free field (flow field of overlapped dimer configuration is divergence-free as we have seen in Eq 2.4), and scaling relation Eq.2.9 for contour lines will be applicable here also.

Let P(s) denote the probability of occurrence of loop of size s when we randomly pick a loop from the set of non-intersecting loops formed after super-posing two random dimer configurations(it is different from $\tilde{P}(s)$ which denote the probability of loop of size s passing through a given lattice point) and

$$P(s) \sim s\tilde{P}(s), \tag{2.10}$$

therefore

$$P(s) \sim \frac{1}{s^{\tau}}, \tag{2.11}$$

and since our system is finite, there will be s_{cutoff} upto which the above power law persist.

$$s_{cutoff} \sim L^{D_f}, \tag{2.12}$$

where, D_f is the fractal dimension. Using the finite size scaling idea ([14],[15]) we propose the following scaling relation for the probability of loop:

$$P(s, L) \sim \frac{1}{L^{D_f\tau}}\tilde{\phi}(\frac{s}{L^{D_f}}), \tag{2.13}$$

where,

$$\tilde{\phi}(x) \sim \frac{1}{x^{\tau}}\ , \ for\ x << 1,$$
$$L = lattice\ size.$$

In the case of random dimer model on square lattice, ζ =0 and since x_1=$\frac{1}{2}$ is universal, we expect from Eq.2.9,

$$\tau \;=\; \frac{7}{3}\,,\;\; D_f \;=\; \frac{3}{2}. \tag{2.14}$$

2.5 Numerical Result

With the help of the worm algorithm (we will discuss in chapter 3) one can generate a new dimer configuration starting from a given dimer configuration. The following algorithm was used to generate non-intersecting loops of random dimer overlap:

1 Starting from the configuration when all the dimers are horizontal, we let the system to go through 2000 worm runs to get a new dimer configuration.

2 An ensemble of 100 such new random dimer configurations was created.

3 Two dimer configurations were randomly chosen from the ensemble of 100, and we let 10 worm runs on each of them. The two new dimer configuration thus generated was overlapped to get the statistics of loops.

4 Step 3 was iterated for 10^7 times.

When two random dimer configurations are overlapped, then the fraction of overlapping dimer should be 0.25, and by the algorithm mentioned above, we were able to maintain this at every step.

Also, while calculating P(s), we used two ways

- ratio of average : after each two random dimer overlap, loop generated were binned according to their lengths, and the total number of loops generated after each iteration was noted. At the end of 10^7 iteration, P(s) was calculated as

$$P(s) \;=\; \frac{total\ number\ of\ loops\ of\ size\ s}{total\ number\ of\ loops\ generated}. \tag{2.15}$$

- average of ratio : after each two random dimer overlap, instead of binning number of loop of specific size s, their probability $p_i(s)$ was binned,

$$p_i(s) \;=\; \frac{number\ of\ subloops\ of\ size\ s\ in\ i^{th}\ iteration}{total\ number\ of\ subloops\ generated\ in\ i^{th}\ iteration}, \tag{2.16}$$

  at the end of n = 10^7 iteration we average $p_i(s)$ to get P(s):

$$P(s) \;=\; \frac{\sum_i (p_i(s))}{n}.$$

We found that the probability derived by both the methods is identical as the distribution of denominator, i.e., the number of subloops generated in each iteration is well-behaved and gaussian (fig 2.6).

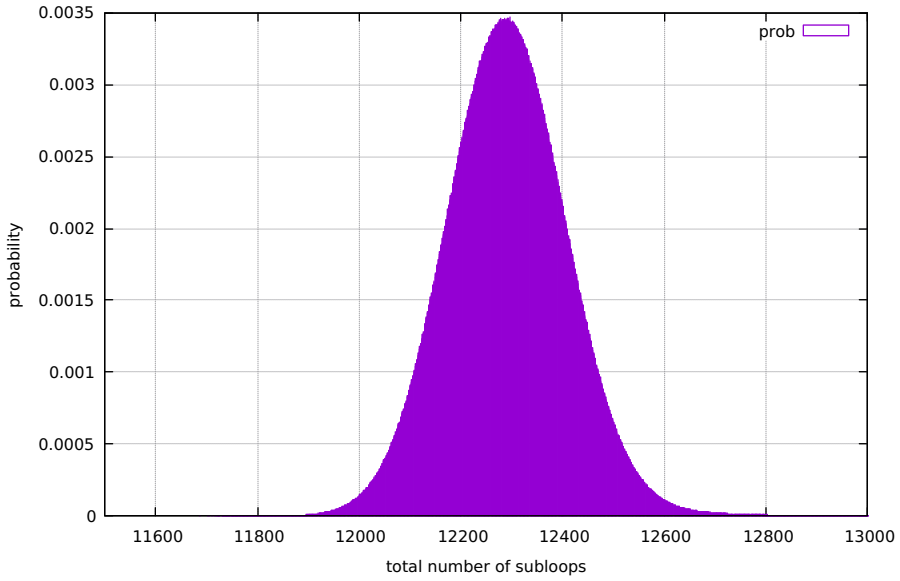

Figure 2.6: Probability distribution of the 'total number of subloops' generated in each iteration when two random dimer configurations are overlapped , L=256

2.5.1 Non-winding subloops

These are the loop of winding number zero. As mentioned earlier, we try to find the exponents τ and D_f using the scaling relation Eq. 2.13. We have plotted log(P(s,L)) vs log(s). So, the

slope of straight-line portion of the curve will give us τ and scaling collapse of the curve of different lattice sizes will give us D_f.

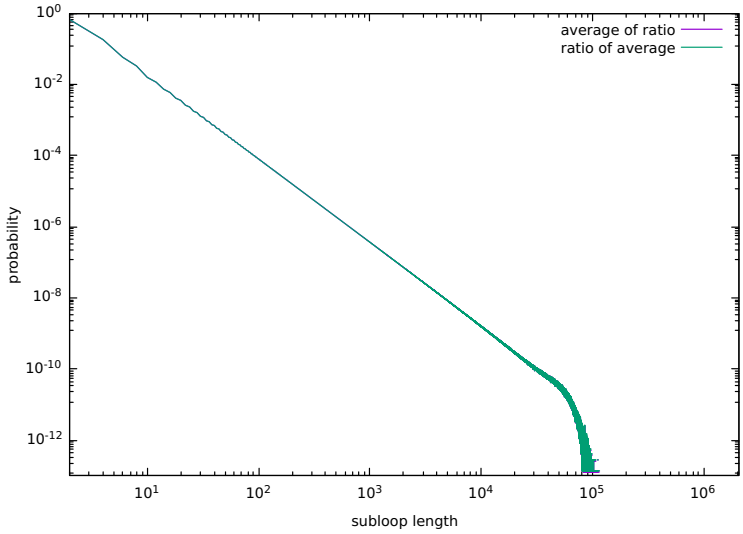

Figure 2.7: Probability distribution of non-winding subloops of overlap dimer configuration calculated by both the method, average of ratio and ratio of average, on a log-log scale. the plot is exactly same, L=1024

The difference between the slope of log(probability) vs log(s) distribution and log(cumulative probability) vs log(s) distribution is exactly one as expected but the data looks more clear in the cumulative probability case, so we have plotted both. Cumulative Probability(s) = $\sum_s^\infty P(s)$.

From Fig 2.8, slope gives us,

$$\tau \ = \ 2.33 + -0.02,$$

which correctly matches the analytical result predicted Eq. 2.14.

2.5.2 Winding Loops

These are the loops with winding numbers non-zero. The length of a loop, in this case, is O(L). These loops also followed the same scaling relation, and scaling collapse of the curve of different lattice sizes gives us the same exponents as in the case of a non-winding loop.

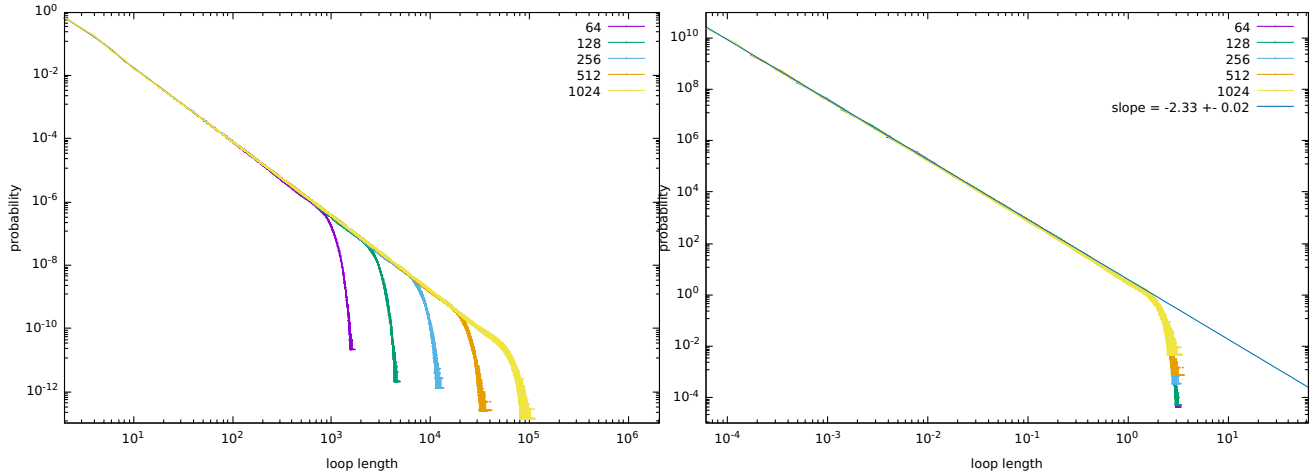

(a) (b)

Figure 2.8: Probability distribution of non-winding subloops on a log-log scale, In fig (b) P(s,L)$L^{D_f\tau}$ vs $\frac{s}{L^{D_f}}$ is plotted

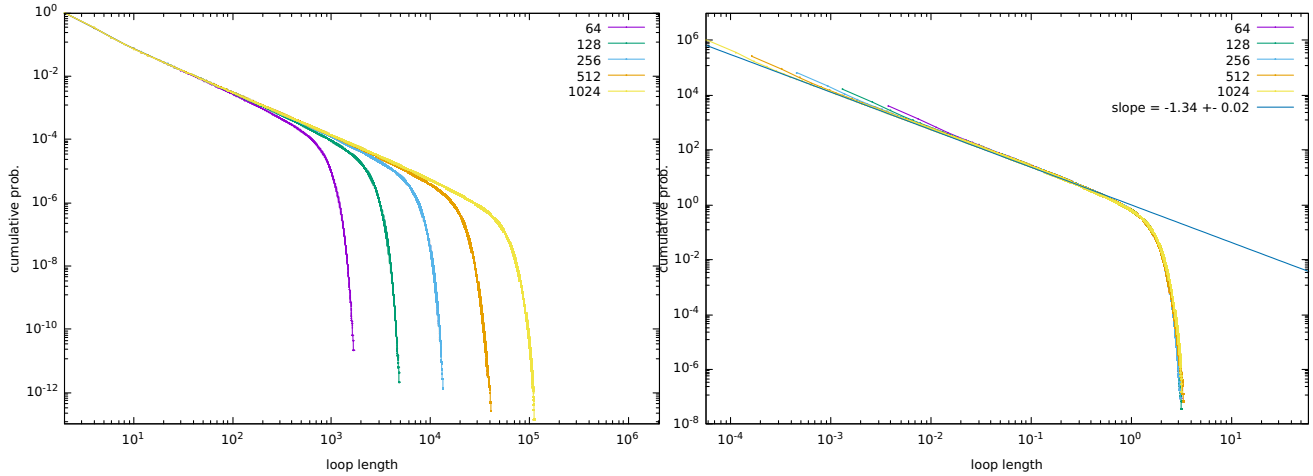

(a) (b)

Figure 2.9: Cumulative probability distribution of non-winding subloops on a log-log scale, fig b is the scaling collapse

Exponents D_f from the collapse of both winding and non-winding loops is precisely identical,

$$D_f \;=\; 1.5 \pm 0.01.$$

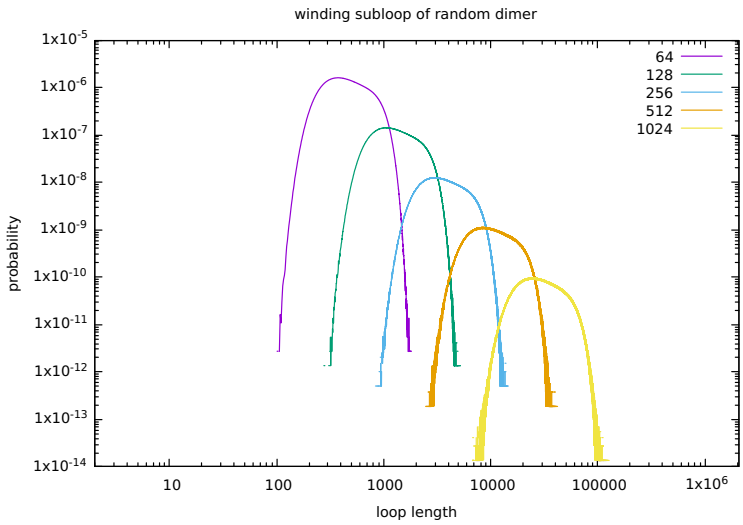

Figure 2.10: Probability distribution of winding subloops of overlap dimer configuration on a log-log scale

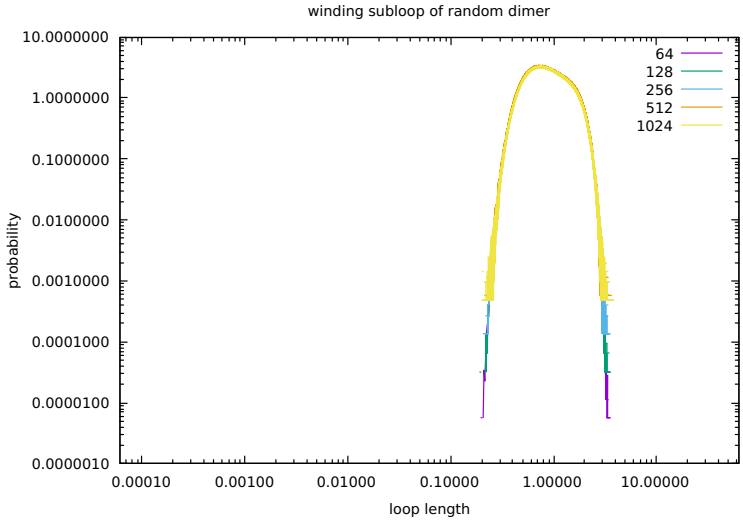

Figure 2.11: Scaling collapse of the probability distribution of winding loop, Here I have plotted $P(s,L)L^{D_f\tau}$ vs $\tilde{\phi}(\frac{s}{L^{D_f}})$ on a log-log scale

Flux

We also looked at the distribution of overall Flux when two random dimer configurations are overlapped. Since our lattice is bipartite, we colour the vertices as green and white such

that all neighbour of a white vertex is green and vice versa. And we assume the orientation that if we start at a white site and measure the flux of a loop, we call the flux positive, and if we start at a green site and measure the flux, we call the flux negative.

Probability distribution of Flux comes out to be gaussian. Let $\beta_x(i)$ denote the flux 'i' in x-direction, i ϵ $\mathbb{Z}$. The distribution of flux is determined by the stiffness K of the field and for random dimer overlap, it was shown in [16] that K = 0.785,

$$\beta_x(i) \sim e^{-K\,(i^2)}. \tag{2.17}$$

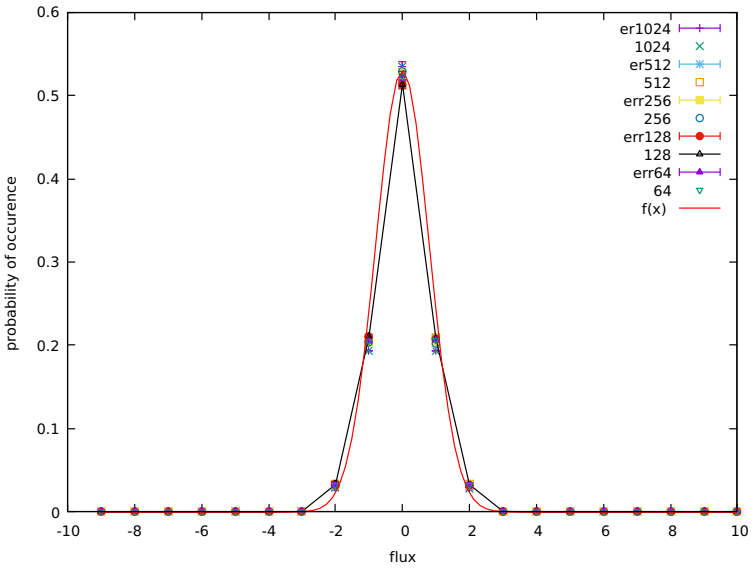

Figure 2.12: Probability distribution of flux

From the simulation, we get K = 0.78 $\pm$ 0.01, closely matching the predicted result.

Chapter 3

The Worm Algorithm

The Worm Algorithm provides an exemplary method for generating non-local updates in Monte Carlo simulation of several lattice models(Sec 5.1 of [17] serves as a brief review). The algorithm starts with the formation of a defect anti-defect pair. The anti-defect traverse through the lattice updating related variable in such a way that detailed balance is maintained at every step. The algorithm ends when the anti-defect reaches the defect and annihilates it.

In a Fully packed dimer model, defects are those lattice points where no dimer is present, and anti-defect are those where two dimers are touching.

The steps of the Worm Algorithm are stated below :

1 Consider a fully packed dimer configuration on a square lattice.

2 Choose a random lattice point; a dimer will be attached to that point.

3 Considering that point as a pivot, rotate the dimer randomly in one of the four directions.(Fig 3.1(a))

4 If the dimer didn't change its position at the first step, we say the worm has backtracked, and its length is 2. There is no change in dimer configuration.

5 If the dimer gets rotated to one of the unoccupied links, then a defect is created at the other end of starting dimer position(Fig 3.1(b) red dot), and an anti-defect(Fig 3.1(b)

blue dot) is created at the other end of the new dimer position. Defect forms at the tail of a worm and remain fixed during worm run, and anti-defect forms at the head of a worm.

6 Then, go to the other end of the anti-defect, connected via the existing dimer. Using it as a pivot now, rotate the dimer. In this way, the head of the worm, i.e., anti-defect keeps moving in the system.

7 Keep repeating step 6 until the worm's head reaches its tail, i.e., anti-defect annihilate the defect created at the start. Keep track of the number of links crossed, and this gives us the length of the worm.(Fig 3.1(c) and 3.1(d))

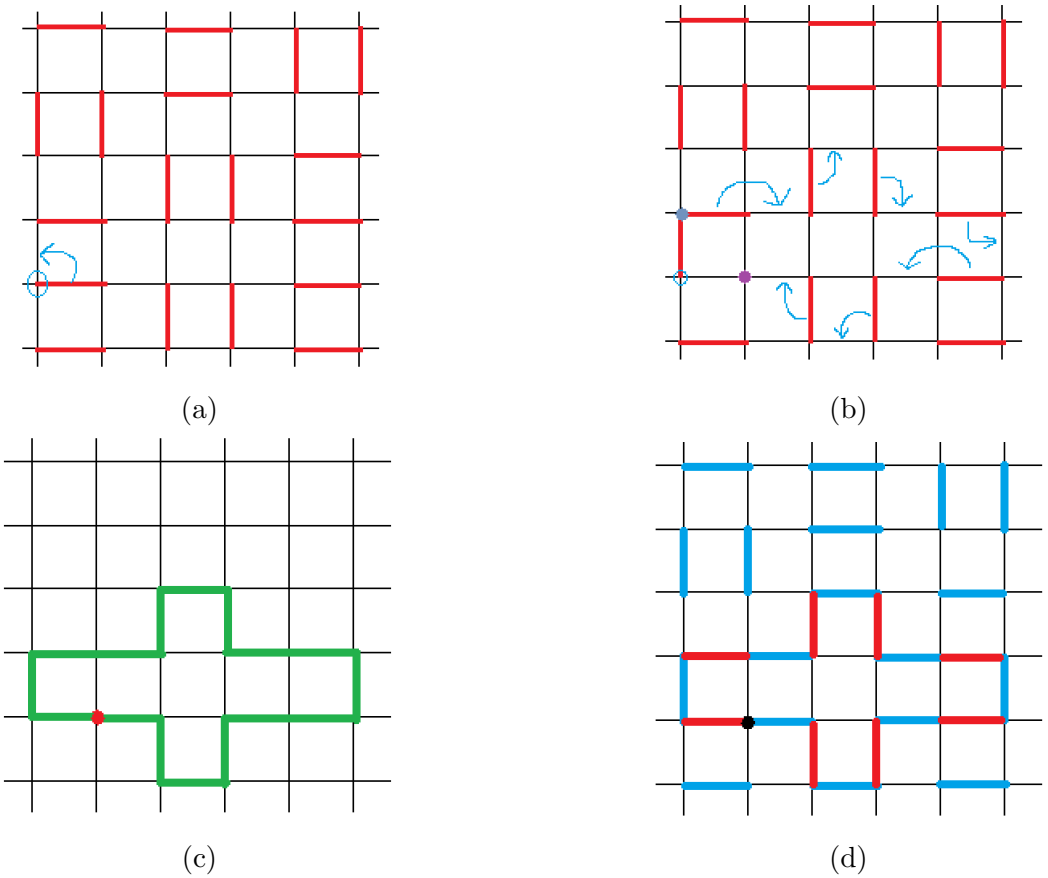

Figure 3.1: Worm Algorithm

3.1 The Worm as a Random Walker

Considering each step of worm formation as position increment of random walker, worm can be seen as random walk in background potential. Random walk in a logarithmic attractive potential in dimension d can be studied as a free random walk in effective dimension d' ([18],[19]),

$$d' \;=\; d - x_1, \tag{3.1}$$

where x_1 is the coefficient of log potential and qualitatively represents the strength of the potential. In our case, it is the universal power-law exponent of the equilibrium defect-antidefect correlation function of the dimer model.

We can then think of the worm's length as the first return time of the random walker. The probability distribution of first return time is a power law for a markovian random walker (walker with no memory). Based on this, we assume

$$P(s) \;\sim\; \frac{1}{s^{1+\theta}}, \tag{3.2}$$

where s is worm length, P(s) is probability that the length of the worm is s in the next iteration and θ is the persistent exponent.
Since we are working in finite system, this power law will persist upto some s_{cutoff}, Let

$$s_{cutoff} \;\sim\; L^z, \tag{3.3}$$

where L is System size and z is dynamical exponent. We use finite size scaling idea to propose:

$$P(s, L) \;\sim\; \frac{1}{L^{z(1+\theta)}}\phi(\frac{s}{L^z}), \tag{3.4}$$

where $\phi(x) \;\sim\; \frac{1}{x^{1+\theta}}$ for x small.
In the paper [12], a general scaling relation that relate z with θ has been derived

$$z \;=\; \frac{2 - x_1}{1 - \theta}. \tag{3.5}$$

For markovian random walker (walker with no memory) $z \;=\; 2$ which gives $\theta \;=\; \frac{x_1}{2}$.

While, as it will turn out for our case, $z \neq 2$ and $\theta > \frac{x_1}{2}$, which suggest that worm run is not markovian.

After the super-imposition of the initial and final dimer configuration separated by a worm, we see that the worm decomposes into several daughter loops. The 'number of daughter loops' produced and 'length of daughter loops' show a power-law distribution. Study about them may help us understand the relation between the geometry of the worm and its daughter loop as the worm can be seen as their convolution. In the subsequent section, we will see the numerical result related to winding and non-winding worms and their daughter loops.

3.2 Non - Winding Worms

3.2.1 Worm length

The number of links crossed by the worm gives us the length of the worm. To get the data, we have run the worm on L = 64, 128, 256, 512, 1024. We created the histogram after the worm run, which gives us P(s) vs s. We used Eq.3.4 for scaling collapse and get the exponents z and θ. We have plotted here log(P(s)) vs log(s), and so the slope of straight line gives us the exponent of Eq.3.4.

Slope of straight lines gives us $\theta = 0.34 \pm 0.02$ and scaling collapse gives z = 2.31 ± 0.03. The x_1 is obtained using the scaling relation Eq.3.5, comes out to be 0.48 ± 0.03, which agrees within the error bars with the theoretical value of $\frac{1}{2}$ for non-interacting dimer model. We can see here that $\theta > \frac{x_1}{2}$ and $z > 2$, which suggest that worm is non-markovian in nature. This is not completely unexpected because as the head of the worm moves it is directed by the background dimer configuration. And the worm follow deatiled balance at each step and the background dimer configuration remains in equilibrium. The power law correlation of equilibrium dimer-dimer configuration give rise to correlation between successive steps taken by the worm. Due to this, we effectively see that worm show non-markovian nature.

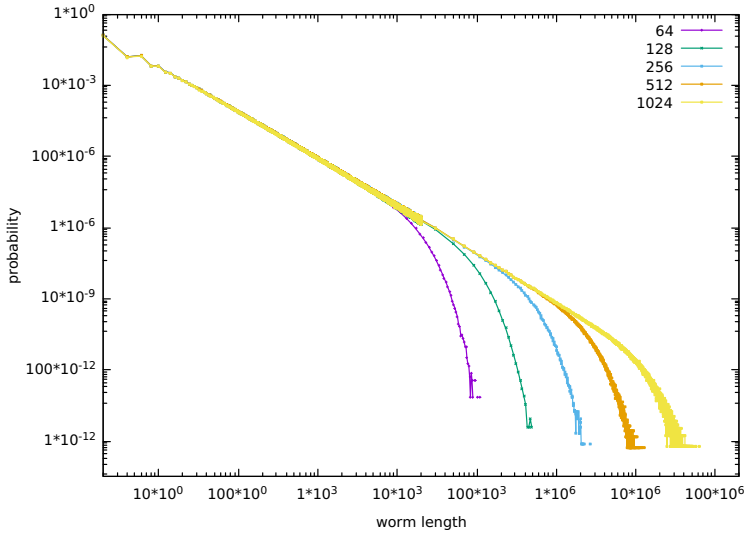

Figure 3.2: Probability distribution of non-winding worm, P(s) vs s is plotted on a log-log scale

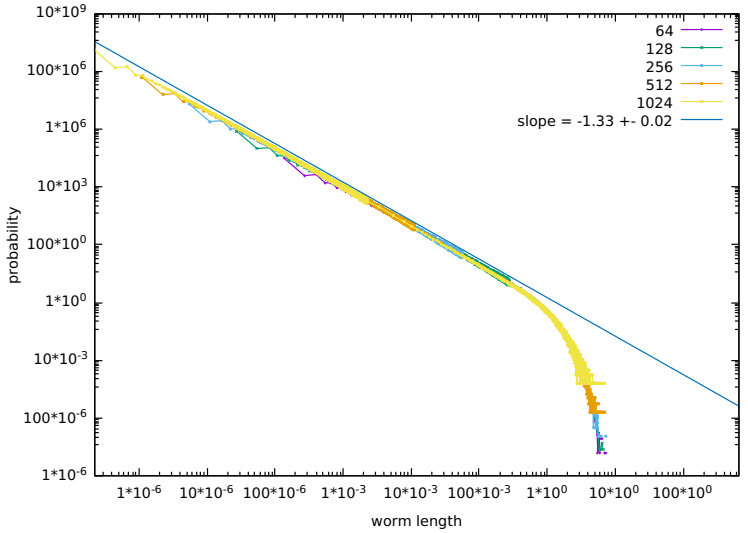

Figure 3.3: Scaling Collapse of the non-winding worms, P(s,L)$L^{z(1+\theta)}$ vs $\frac{s}{L^z}$ is plotted on a log-log scale

3.2.2 Distribution of Subloops

Overlap of consecutive dimer configuration gives us a decomposition of worm in its daughter loops. We looked at the distribution of these subloops and calculated Q(s) (Probability of

occurrence of subloop of size s). We can again calculate Q(s) in two ways: ratio of average (2.5) and average of ratio (2.5) (as was discussed in chapter 2). The distribution comes out to be starkly different, which can be linked to the fact that the distribution of denominator(number of subloops generated after each iteration) of Eq.2.16 is itself power-law distributed (Fig 3.7). The distribution in both the cases follow finite-size scaling relation:

$$Q(s, L) \sim \frac{1}{L^{ab}} \phi(\frac{s}{L^a}), \tag{3.6}$$

where $\phi(x) \sim \frac{1}{x^b}$, for x small; a is fractal exponent and b is persistent exponent of the subloop distribution.

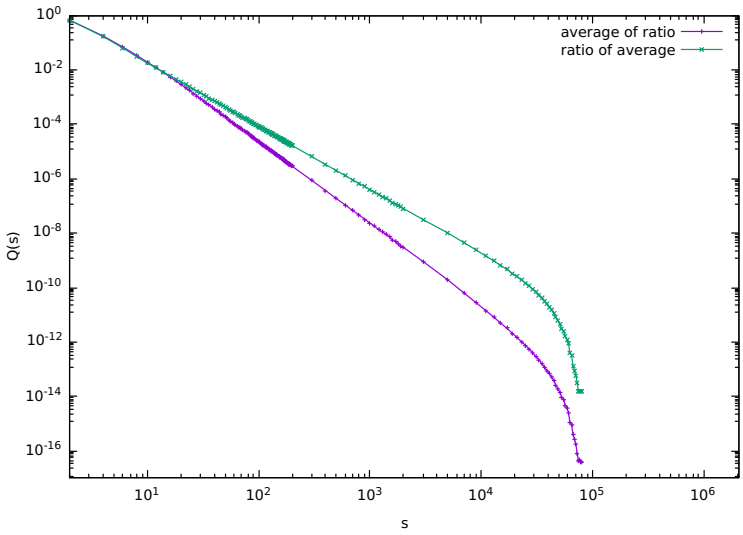

Figure 3.4: Probability distribution of non-winding subloops of the non-winding worm by two different methods, ratio of average and average of ratio,on a log-log scale. The slope in both the case is different from one another.

- ratio of average : Scaling collapse (Fig 3.5 (b)) gives a = 1.5 ± 0.02 which is same D_f of contour loop and b = 2.33 ± 0.03 which is same as τ of contour loop of random gaussian surface.
- average of ratio: Scaling collapse (Fig 3.6 (b)) gives us a = 1.5 ± 0.02 which is same D_f of contour loop but b = 3 ± 0.02 in this case is very different from τ.

The fractal dimension of daughter loop 'a' comes out to be same from both the method while

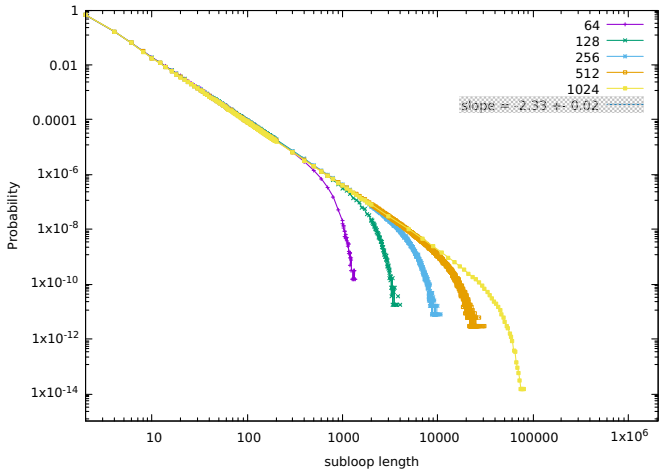

(a)

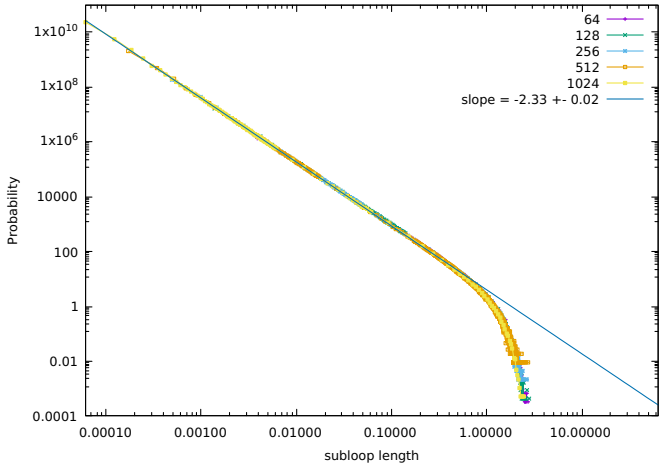

(b)

Figure 3.5: Probability distribution of subloops of non-winding worms (ratio of average method) on a log-log scale, Fig b is the scaling collapse

the persistent exponent 'b' is different.

3.2.3 Distribution of the number of subloops

The probability distribution of 'number of subloops' that a worm breaks into also follows finite-size scaling relation(Fig 3.7). Let $P_N(i)$ denotes the probability of 'number of subloops generated is i after the worm run'.

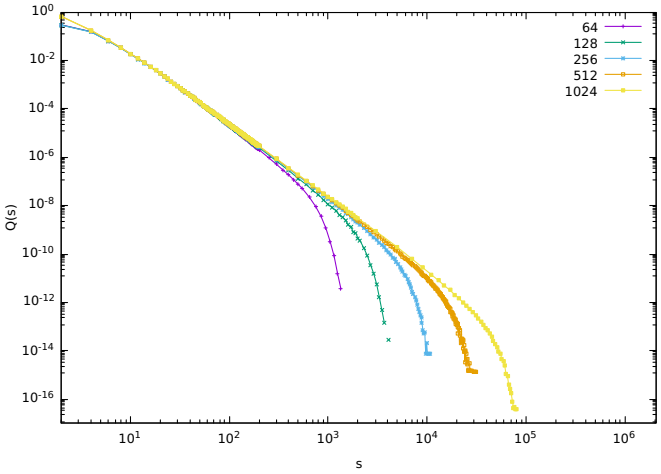

(a)

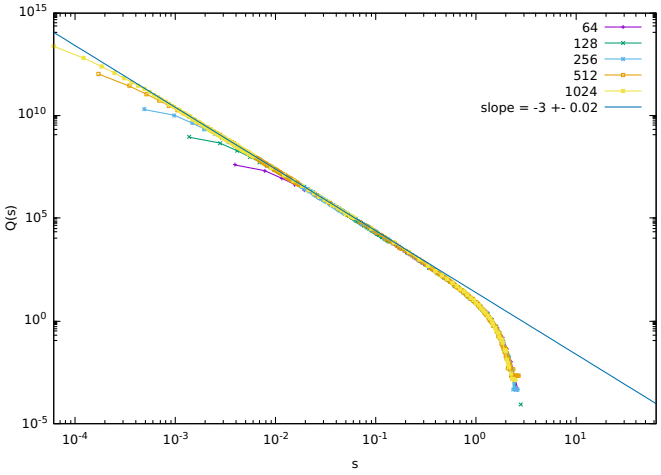

(b)

Figure 3.6: Probability distribution of subloops of non-winding worms(average of ratio method) on a log-log scale, Fig (b) is the scaling collapse

$$P_N(i, L) \sim \frac{1}{L^{cd}} \phi(\frac{i}{L^c}), \tag{3.7}$$

where $\phi(x) \sim \frac{1}{x^d}$, for x small. Scaling collapse gives c = 1.98 ± 0.04 and d = 1.42 ± 0.02.

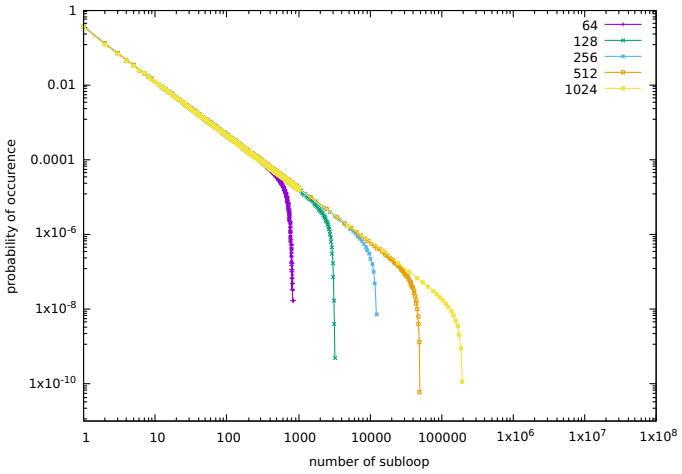

(a)

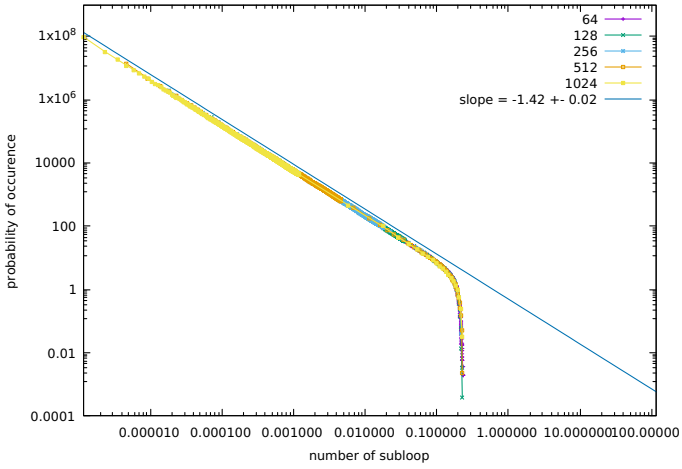

(b)

Figure 3.7: Probability distribution of 'no. of subloops' of non-winding worms on a log-log scale, Fig b is the scaling collapse

3.3 Winding Worms

3.3.1 Worm length

The length of these worms is O(L), where L is lattice size. These worms also follow the finite size relation

$$P(s, L) \sim \frac{1}{L^{z(1+\theta)}} \phi(\frac{s}{L^z}). \tag{3.8}$$

Although, we can not say $\phi(x) \sim \frac{1}{x^{1+\theta}}$ for small x. Scaling collapse gives z = 2.34 ± 0.03

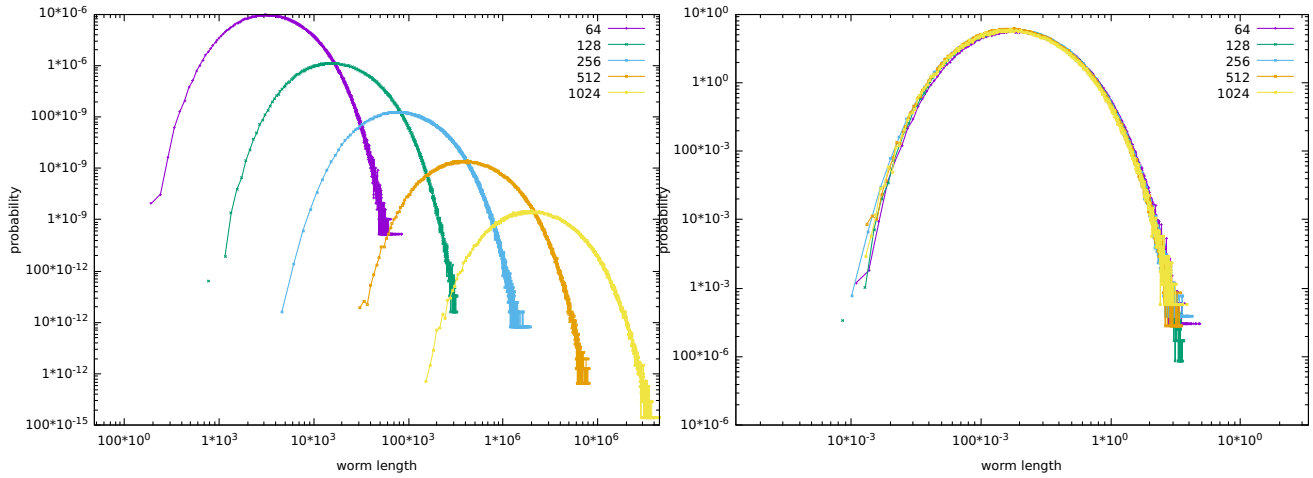

(a) (b)

Figure 3.8: Probability distribution of winding worms, Fig b is the scaling collapse, $\log(\mathrm{P(s},L)L^{z(1+\theta)})$ vs $\log(\frac{s}{L^z})$ is plotted

and $z(1+\theta) = 3.15 \pm 0.04$. Ratio of them gives $\theta = 0.34$ which is same as what we got from the distribution of non-winding worms.

3.3.2 Distribution of Subloops

Since the worm is winding, it can have winding as well as non-winding subloops. The probability distribution of subloops follows finite-size scaling relation Eq 3.6, similar to the subloops of non-winding worms,

$$Q(s,L) \sim \frac{1}{L^{ab}}\phi(\frac{s}{L^a}), \tag{3.9}$$

where $\phi(x) \sim \frac{1}{x^b}$, for x small.
The difference here is that the distribution of Q(s) comes out to be the same for the ratio of average and average of ratio method (Fig 3.9). This can be due to the fact that the distribution of number of subloops generated after each worm is non-monotonic and has a peak (Fig 3.14) compared to the power-law distribution of 'number of subloops' generated in the case of non-winding worms(Fig 3.7).

- non-winding subloops : Scaling collpase Fig (3.10a) and Fig (3.11a) of the curve gives

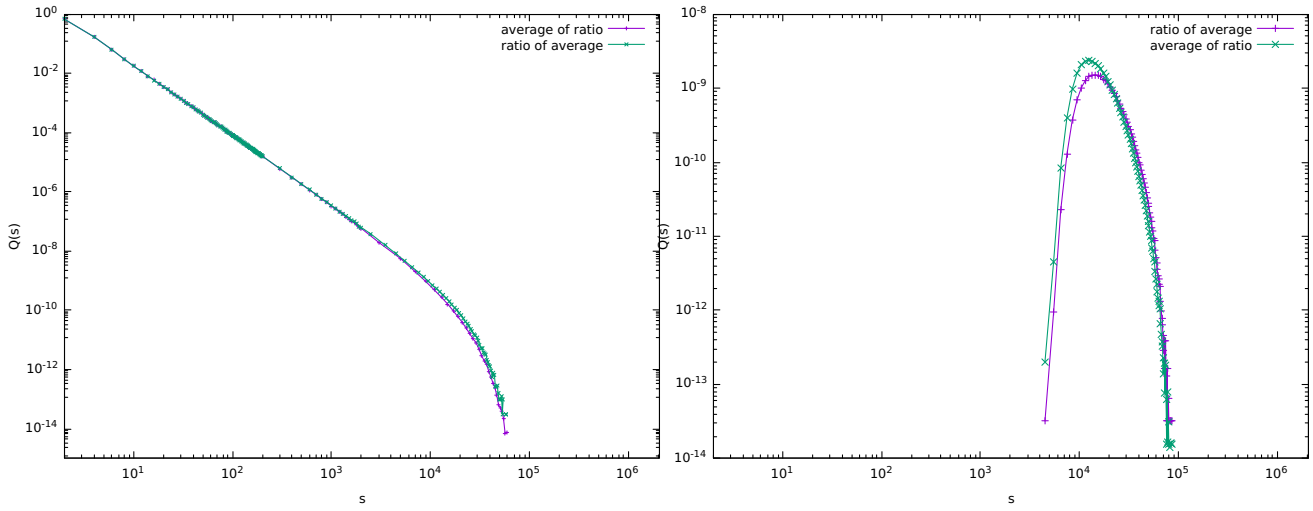

(a) (b)

Figure 3.9: Probability Distribution of subloops of winding worm by both the method on a log-log scale, Fig a is of non-winding subloops, Fig b is of winding subloops

a = 1.5 ± 0.02 and b = 2.33 ± 0.01. These two matches exactly with exponent D_f and τ of contour loop respectively.

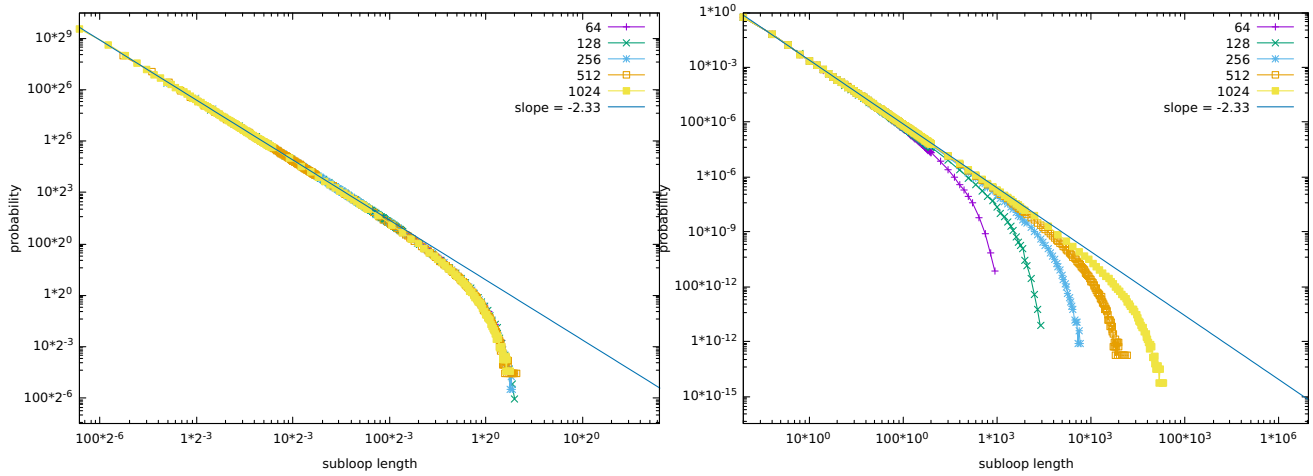

(a) (b)

Figure 3.10: Probability distribution of non-winding subloops of winding worm on a log-log scale, ratio of average method

- winding subloops : Scaling collpase (Fig 3.12b and Fig 3.13b) of the curve gives a = 1.47 ± 0.04 and ab = 3.44 ± 0.03 which gives b = 2.34. The exponent a and b is close

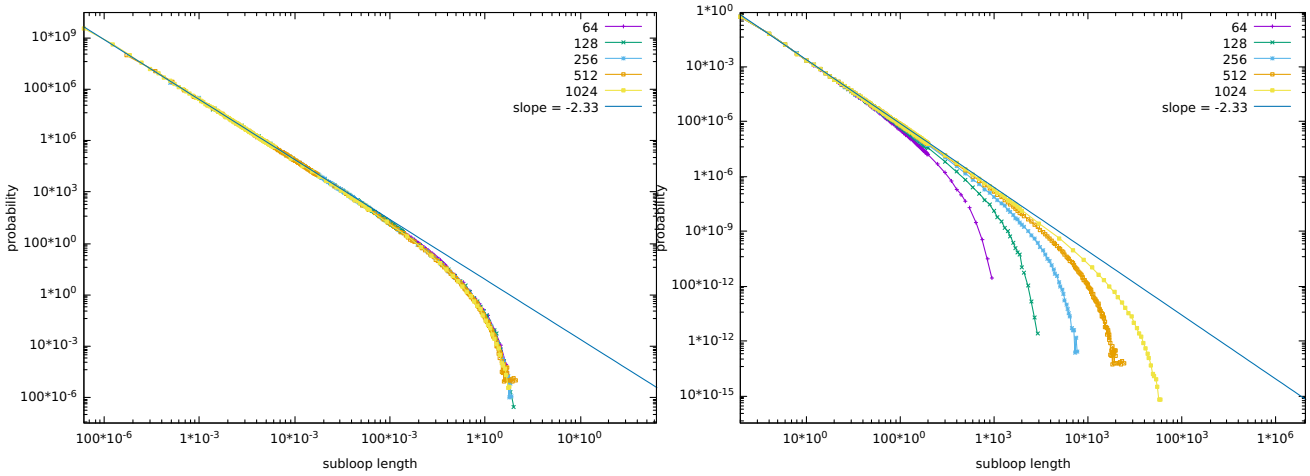

(a) (b)

Figure 3.11: Probability distribution of non-winding subloops of winding worm on a log-log scale, average of ratio method

to D_f and τ of contour loop respectively.

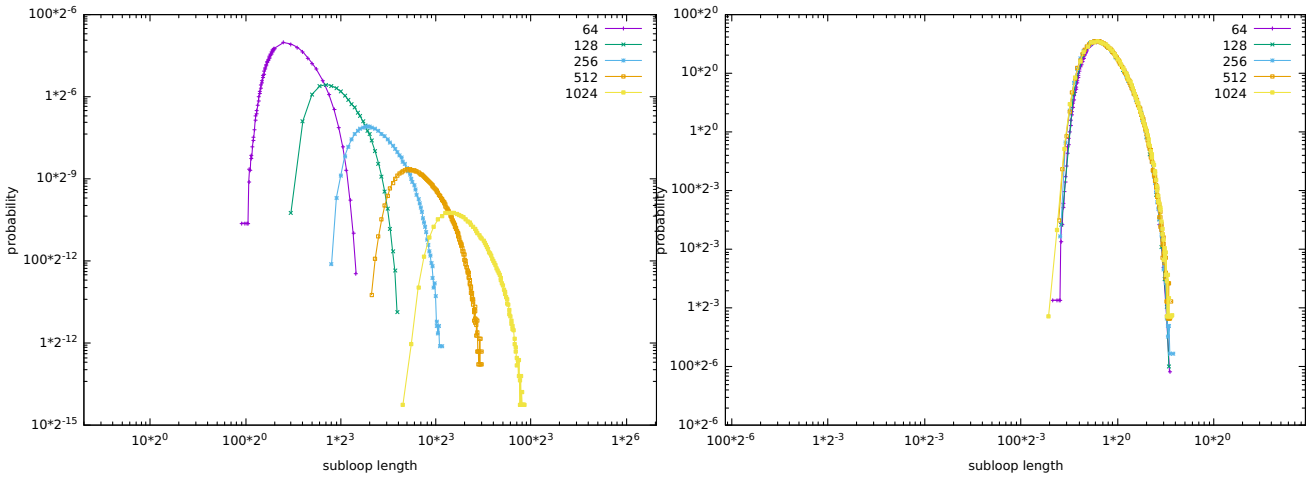

(a) (b)

Figure 3.12: Probability distribution of winding subloops of winding worm on a log-log scale, ratio of average method

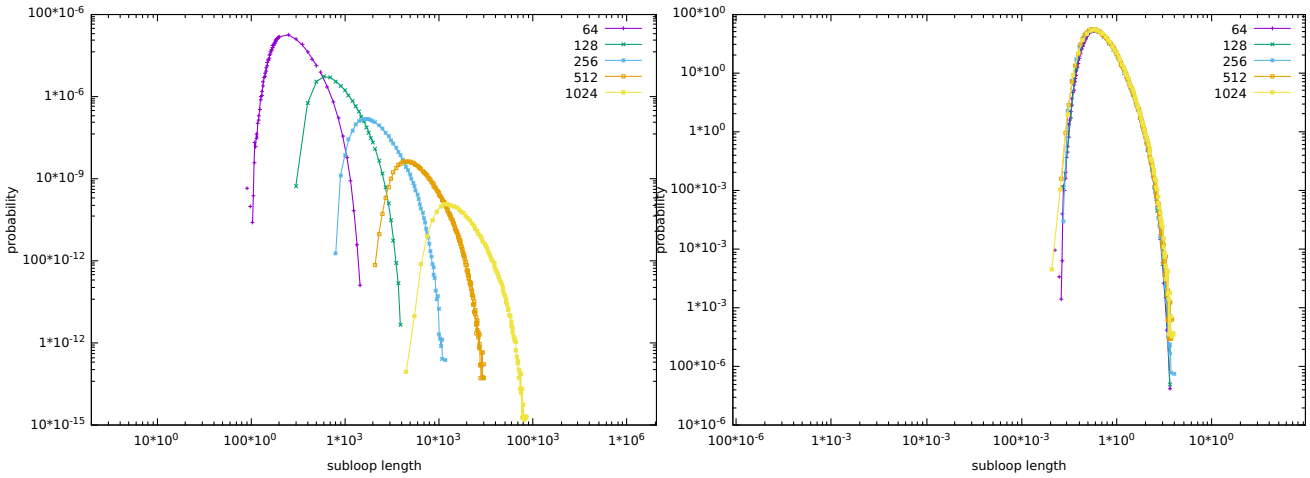

(a) (b)

Figure 3.13: Probability distribution of winding subloops of winding worm on a log-log scale, average of ratio method

3.3.3 Distribution of the number of subloops

The probability distribution of number of subloops that a winding worm breaks into also follows finite-size scaling relation similar to the case of a non-winding worm. Here the distribution is non-monotonic (Fig 3.14).

$$P_N(i, L) \sim \frac{1}{L^{cd}} \phi(\frac{i}{L^c}). \tag{3.10}$$

Scaling collapse gives c = 1.97 ± 0.04 and cd = 2.81 ± 0.02. which gives d = 1.42, same as what we have got from the slope of probability distribution of number of subloops of non-winding worm case on a log-log plot.

3.3.4 Flux distribution

We also looked at the distribution of winding worms based on their flux. The distribution comes out to be similar for both x and y directions as expected. The distribution of overall flux for overlap of two random dimer configurations was gaussian, but for the case of the worm, it comes out to be different. Equation

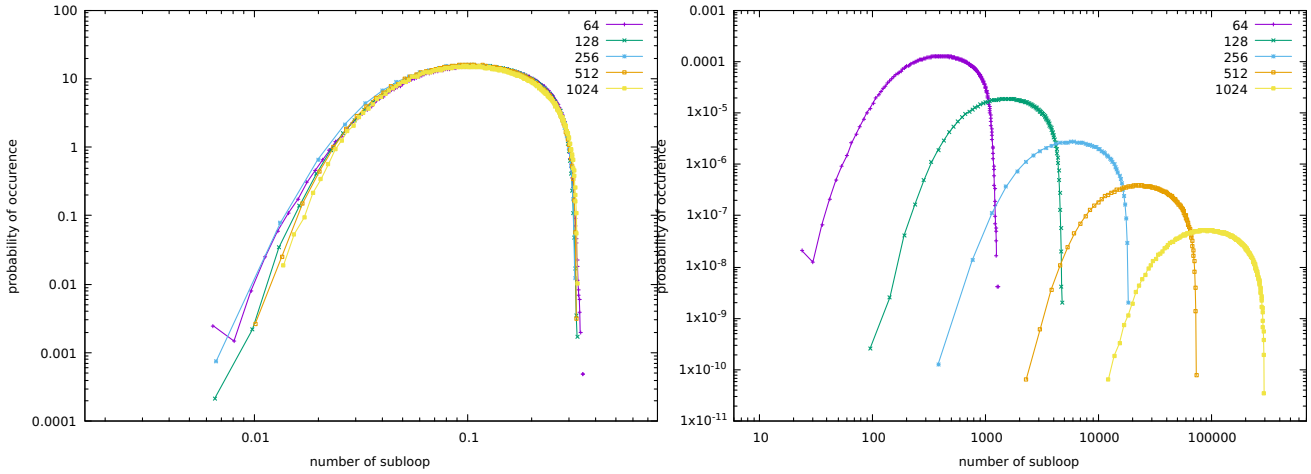

(a) (b)

Figure 3.14: Probability distribution of no. of subloops of a winding worm on a log-log scale

$$\beta_x(i) \sim e^{-p\,(i^4)}, \tag{3.11}$$

(where i is flux, and i ϵ $\mathbb{Z}$) fits the data point and gives p = 0.27 $\pm$ 0.02.

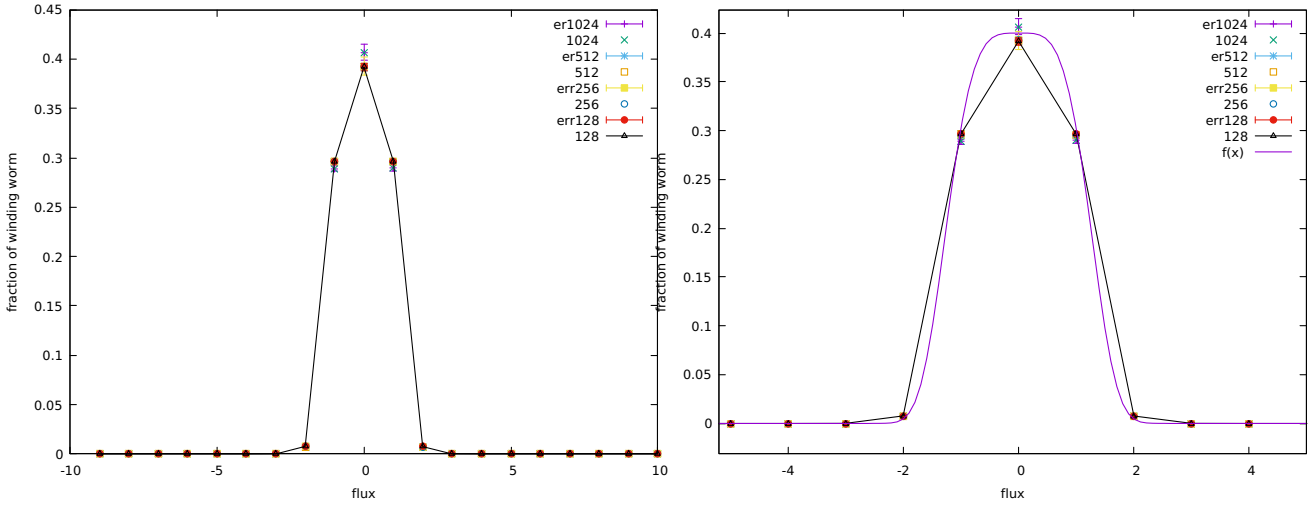

(a) (b)

Figure 3.15: Probability distribution of winding worm with respect to flux

Chapter 4

Conclusion

In chapter 2, we looked at the distribution of subloops when two random dimer configurations are overlapped. We used two methods, namely ratio of average and average of ratio, to obtain the exponents of the subloops distribution. The exponent obtained numerically exactly matches with the analytical prediction based on the mapping of these loops to contour lines of random gaussian surfaces. We also looked at 'Number of Subloops' distribution generated after dimer overlap and found it to be gaussian. The probability distribution of flux when two random dimers are overlapped was also gaussian.

- Exponents characterizing the distribution of subloops when two random dimers are overlapped (Eq. 2.13): $\tau = 2.33 \pm 0.02$ and $D_f = 1.5 \pm 0.01$.

- Distribution of flux gives stiffness (Eq. 2.17) K $= 0.78 \pm 0.01$.

In chapter 3, we looked at the properties of the worm generated by the worm algorithm. When interpreted as a random walker, we found that these worms turn out to be a non-markovian random walk. Next, we looked at the distribution of subloops of a worm. We looked separately at winding worm and non-winding worm. In the case of a non-winding worm, distribution of subloops when seen in two different ways, i.e., ratio of average and average of ratio, comes out to be different. Since, we don't have any analytical solution to verify and we don't know which of the two quantity i.e. probability as ratio of average

or prbability as average of ratio will be easier to model analytically, we have found the numerical results by both the approach. In the case of the winding worm, the distribution of subloops seen by both methods comes out to be the same, and the distribution is similar to the distribution of subloops of random dimer overlap.

- Distribution of length of the worm generated (both winding and non-winding) during the worm algorithm is characterized by two exponents (Eq. 3.4): z = 2.31 ± 0.03 and $\theta = 0.34 \pm 0.02$.
- Distribution of subloops of the non-winding worm:
  - ratio of average method (2.5): $\tau = 2.33 \pm 0.02$ and $D_f = 1.5 \pm 0.02$ similar to the exponents of random dimer overlap.
  - average of ratio method (2.5): $\tau = 3 \pm 0.02$ and $D_f = 1.5 \pm 0.02$, difference in the value of τ is due to the fact that 'number of subloops' that a worm breaks into is itself power-law distributed and follows a scaling relation (Eq. 3.7).
- Distribution of subloops of winding worm:
  - $\tau = 2.33 \pm 0.02$ and $D_f = 1.5 \pm 0.02$ similar to the exponents of random dimer overlap from both the ratio of average and average of ratio method.
- Exponents characterizing the distribution of 'number of subloops' (Eq. 3.7): persistent exponent = 1.42 ± 0.02 and dynamical exponent = 1.98 ± 0.04.

In future work, it would be interesting to establish the relation between the exponents characterizing the distribution of worms and distribution of subloops and 'no. of subloops' that a worm breaks into. We have looked at the case where there is no interaction between the dimers other than the usual dimer constraint; more interesting work can be carried out by taking into account different interactions between the dimers.

Bibliography

[1] R. H. Fowler and G. S. Rushbrooke, "An attempt to extend the statistical theory of perfect solutions," *Trans. Faraday Soc.*, 1937. [Online]. Available: http://dx.doi.org/10.1039/TF9373301272

[2] P. Kasteleyn, "The statistics of dimers on a lattice: I. the number of dimer arrangements on a quadratic lattice," *Physica*, 1961. [Online]. Available: https://www.sciencedirect.com/science/article/pii/0031891461900635

[3] H. N. V. Temperley and M. E. Fisher, "Dimer problem in statistical mechanics-an exact result," *The Philosophical Magazine: A Journal of Theoretical Experimental and Applied Physics*, 1961. [Online]. Available: https://doi.org/10.1080/14786436108243366

[4] M. E. Fisher and J. Stephenson, "Statistical mechanics of dimers on a plane lattice. ii. dimer correlations and monomers," *Phys. Rev.*, 1963. [Online]. Available: https://link.aps.org/doi/10.1103/PhysRev.132.1411

[5] M. E. Fisher, "On the dimer solution of planar ising models," *Journal of Mathematical Physics*. [Online]. Available: https://doi.org/10.1063/1.1704825

[6] D. S. Rokhsar and S. A. Kivelson, "Superconductivity and the quantum hard-core dimer gas," *Phys. Rev. Lett.*, 1988. [Online]. Available: https://link.aps.org/doi/10.1103/PhysRevLett.61.2376

[7] W. P. Thurston, "Conway's tiling groups," *The American Mathematical Monthly*, 1990. [Online]. Available: http://www.jstor.org/stable/2324578

[8] F. Alet, Y. Ikhlef, J. L. Jacobsen, G. Misguich, and V. Pasquier, "Classical dimers with aligning interactions on the square lattice," *Phys. Rev. E*, 2006. [Online]. Available: https://link.aps.org/doi/10.1103/PhysRevE.74.041124

[9] S. Papanikolaou, E. Luijten, and E. Fradkin, "Quantum criticality, lines of fixed points, and phase separation in doped two-dimensional quantum dimer models," *Phys. Rev. B*, 2007. [Online]. Available: https://link.aps.org/doi/10.1103/PhysRevB.76.134514

[10] H. W. J. Blote and H. J. Hilborst, "Roughening transitions and the zero-temperature triangular ising antiferromagnet," *Journal of Physics A: Mathematical and General*, 1982. [Online]. Available: https://doi.org/10.1088/0305-4470/15/11/011

[11] B. Nienhuis, H. J. Hilhorst, and H. W. J. Blote, "Triangular SOS models and cubic-crystal shapes," *Journal of Physics A: Mathematical and General*, 1984. [Online]. Available: https://doi.org/10.1088/0305-4470/17/18/025

[12] G. Rakala, K. Damle, and D. Dhar, "Fractional brownian motion of worms in worm algorithms for frustrated ising magnets," *Phys. Rev. E*, 2021. [Online]. Available: https://link.aps.org/doi/10.1103/PhysRevE.103.062101

[13] J. Kondev and C. L. Henley, "Geometrical exponents of contour loops on random gaussian surfaces," 1995. [Online]. Available: https://journals.aps.org/prl/abstract/10.1103/PhysRevLett.74.4580

[14] M. Fisher, "Proceedings of the enrico fermi international school of physics," 1971.

[15] M. E. Fisher and M. N. Barber, "Scaling theory for finite-size effects in the critical region," *Phys. Rev. Lett.*, 1972. [Online]. Available: https://link.aps.org/doi/10.1103/PhysRevLett.28.1516

[16] R. Raghavan, C. L. Henley, and S. L. Arouh, "New two-color dimer models with critical ground states," *Journal of Statistical Physics*, 1997. [Online]. Available: http://dx.doi.org/10.1007/BF02199112

[17] H. G. Evertz, "The loop algorithm," *Advances in Physics*, 2003. [Online]. Available: https://doi.org/10.1080/0001873021000049195

[18] A. J. Bray, "Random walks in logarithmic and power-law potentials, nonuniversal persistence, and vortex dynamics in the two-dimensional XY model," *Phys. Rev. E*, 2000. [Online]. Available: https://link.aps.org/doi/10.1103/PhysRevE.62.103

[19] S. Redner, "A guide to first-passage processes cambridge university press, cambridge, uk, 2001."